

A Statistical Dynamical Model to Predict Extreme Events and Anomalous Features in Shallow Water Waves with Abrupt Depth Change

Andrew J. Majda^{a,1}, M. N. J. Moore^b, and Di Qi^{a,1}

^aDepartment of Mathematics and Center for Atmosphere and Ocean Science, Courant Institute of Mathematical Sciences, New York University, New York, NY 10012;

^bDepartment of Mathematics and Geophysical Fluid Dynamics Institute, Florida State University, Tallahassee, FL

This manuscript was compiled on November 27, 2018

Understanding and predicting extreme events and their anomalous statistics in complex nonlinear systems is a grand challenge in climate, material, and neuroscience, as well as for engineering design. Recent controlled laboratory experiments in weakly turbulent shallow water with abrupt depth change (ADC) exhibit a remarkable transition from nearly Gaussian statistics in incoming wave trains before the ADC to outgoing waves trains after the ADC with extreme anomalous statistics with large positive skewness of the surface height. Here we develop a statistical dynamical model to explain and quantitatively predict the above anomalous statistical behavior as experimental control parameters are varied. The first step is to use incoming and outgoing truncated Korteweg-de Vries (TKdV) equations matched in time at the ADC. The TKdV equation is a Hamiltonian system which induces incoming and outgoing statistical Gibbs invariant measures. The statistical matching of the known nearly Gaussian incoming Gibbs state at the ADC completely determines the predicted anomalous outgoing Gibbs state, which can be calculated by a simple sampling algorithm, verified by direct numerical simulations, and successfully captures key features of the experiment. There is even an analytic formula for the anomalous outgoing skewness. The strategy here should be useful for predicting extreme anomalous statistical behavior in other dispersive media in different settings (21, 22).

extreme anomalous event | statistical TKdV model | matching Gibbs measures | surface wave displacement and slope

Understanding and predicting extreme events and their anomalous statistics in complex nonlinear systems is a grand challenge in climate, material and neuroscience as well as for engineering design. This is a very active contemporary topic in applied mathematics with qualitative and quantitative models (1–7) and novel numerical algorithms which overcome the curse of dimensionality for extreme event prediction in large complex systems (2, 8–11). The occurrence of Rogue waves as extreme events within different physical settings of deep water (12–16) and shallow water (17–19) is an important practical topic.

Recent laboratory experiments in weakly turbulent shallow water reveal a remarkable transition from Gaussian to anomalous behavior as surface waves cross an abrupt depth change (ADC). A normally-distributed incoming wave train, upstream of the ADC, transitions to a highly non-Gaussian outgoing wave train, downstream of the ADC, that exhibits large positive skewness of the surface height and more frequent extreme events (20). Here we develop a statistical dynamical model to explain and quantitatively predict this anomalous behavior as experimental control parameters are varied. The first step is to use incoming and outgoing truncated Korteweg-de Vries (TKdV) equations matched in time at the ADC. The TKdV

equation is a Hamiltonian system which induces incoming and outgoing Gibbs invariant measures. The statistical matching of the known nearly Gaussian incoming Gibbs state at the ADC completely determines the predicted anomalous outgoing Gibbs state, which can be calculated by a simple MCMC algorithm, verified by direct numerical simulations, and successfully captures key features of the experiment. There is even an analytic formula for the anomalous outgoing skewness. The strategy here should be useful for predicting extreme anomalous statistical behavior in other dispersive media in different settings (21, 22).

1. Experiments showing anomalous wave statistics induced by an abrupt depth change

Controlled laboratory experiments were carried out in (20) to examine the statistical behavior of surface waves crossing an ADC. In these experiments, nearly unidirectional waves are generated by a paddle wheel and propagate through a long, narrow wave tank. Midway through, the waves encounter a step in the bottom topography, and thus abruptly transition to a shallower depth. The paddle wheel is forced with a pseudo-random signal intended to mimic a Gaussian random sea upstream of the ADC. In particular, the paddle angle is

Significance Statement

Understanding and predicting extreme events and their anomalous statistics in complex nonlinear systems is a grand challenge in applied sciences as well as for engineering design. Recent controlled laboratory experiments in weakly turbulent shallow water with abrupt depth change exhibit a remarkable transition from nearly Gaussian statistics to extreme anomalous statistics with large positive skewness of the surface height. We develop a statistical dynamical model to explain and quantitatively predict the anomalous statistical behavior. The incoming and outgoing waves are modeled by the truncated Korteweg-de Vries equations statistically matched at the depth change. The statistical matching of the known nearly Gaussian incoming Gibbs state completely determines the predicted anomalous outgoing Gibbs state, and successfully captures key features of the experiment.

A.J.M. designed the research. A.J.M., M.N.J.M., and D.Q. performed the research. A.J.M., M.N.J.M., and D.Q. wrote the paper.

The authors declare no conflict of interest.

¹To whom correspondence should be addressed. E-mail: qidi@cims.nyu.edu, jonjon@cims.nyu.edu

125 specified as

$$126 \quad \theta(t) = \theta_0 + \Delta\theta \sum_{n=1}^N a_n \cos(\omega_n t + \delta_n), \quad E \sim (\Delta\theta)^2 \sum_n a_n^2 \omega_n^2.$$

130 where the weights a_n are Gaussian in spectral space with
 131 peak frequency ω_p and the phases δ_n are uniformly distributed
 132 random variables. The peak frequency gives rise to a char-
 133 acteristic wavelength λ_c which can be estimated from the
 134 dispersion relation. The energy E injected into the system
 135 is determined by the angle amplitude $\Delta\theta$, which is the main
 136 control parameter varied in (20). Optical measurements of the
 137 free surface reveal a number of surprising statistical features:

- 138 • Distinct statistics are found between the incoming and
 139 outgoing wave disturbances: incoming waves display near-
 140 Gaussian statistics, while outgoing waves skew strongly
 141 towards positive displacement.
- 142 • The degree of non-Gaussianity present in the outgoing
 143 waves depends on the injected energy E : larger energies
 144 generate stronger skewness in the surface displacement
 145 PDFs and more extreme events.
- 146 • Compared to the incoming wave train, the power spectrum
 147 of the outgoing wave field decays more slowly, which
 148 indicates that the anomalous behavior is associated with
 149 an elevated level of high frequencies.

152 2. Surface wave turbulence modeled by truncated KdV 153 equation with depth dependence

155 The Korteweg-de Vries (KdV) equation (23) is a leading-order
 156 approximation of surface waves that are determined by the
 157 balance of nonlinear and dispersive effects in an appropriate
 158 far-field limit. Here, the KdV equation is truncated in the first
 159 Λ modes (with $J = 2\Lambda + 1$ grid points) to generate weakly
 160 turbulent dynamics. The surface displacement is described
 161 by the state variable $u_\Lambda^\pm(x, t)$ with superscript ‘–’ for the
 162 incoming waves and ‘+’ for the outgoing waves. The Galerkin
 163 truncated variable $u_\Lambda = \sum_{1 \leq |k| \leq \Lambda} \hat{u}_k(t) e^{ikx}$ is normalized
 164 with zero mean $\hat{u}_0 = 0$ and unit energy $2\pi \sum_{k=1}^\Lambda |\hat{u}_k|^2 = 1$,
 165 which are conserved quantities, and $u_\Lambda \equiv \mathcal{P}_\Lambda u$ denotes the
 166 subspace projection. The evolution of u_Λ^\pm is governed by the
 167 truncated KdV equation with depth change D_\pm

$$168 \quad \frac{\partial u_\Lambda^\pm}{\partial t} + \frac{D_\pm^{-3/2}}{2} E_0^{1/2} L_0^{-3/2} \frac{\partial}{\partial x} \mathcal{P}_\Lambda (u_\Lambda^\pm)^2 + D_\pm^{1/2} L_0^{-3} \frac{\partial^3 u_\Lambda^\pm}{\partial x^3} = 0. \quad [1]$$

172 Equation [1] is non-dimensionalized on the periodic domain
 173 $x \in [-\pi, \pi]$. The depth is assumed to be unit $D_- = 1$ before
 174 the ADC and becomes $D_+ < 1$ after the ADC. The conserved
 175 Hamiltonian can be decomposed into a cubic and a quadratic
 176 term

$$177 \quad \mathcal{H}_\Lambda^\pm = D_\pm^{-3/2} E_0^{1/2} L_0^{-3/2} H_3(u_\Lambda^\pm) - D_\pm^{1/2} L_0^{-3} H_2(u_\Lambda^\pm),$$

$$178 \quad H_3(u) = \frac{1}{6} \int_{-\pi}^{\pi} u^3 dx, \quad H_2(u) = \frac{1}{2} \int_{-\pi}^{\pi} \left(\frac{\partial u}{\partial x} \right)^2 dx.$$

182 We introduce parameters (E_0, L_0, Λ) based on the following
 183 assumptions:

- 184 • The wavenumber truncation Λ is fixed at a moderate
 185 value for generating weakly turbulent dynamics;

- 187 • The state variable u_Λ^\pm is normalized with zero mean and
 188 unit energy, $\mathcal{M}(u_\Lambda) = 0, \mathcal{E}(u_\Lambda) = 1$, which are conserved
 189 during evolution. Meanwhile, E_0 characterizes the total
 190 energy injected into the system based on the driving
 191 amplitude $\Delta\theta$;

- 192 • The length scale of the system L_0 is chosen so that the
 193 resolved scale $\Delta x = 2\pi L_0/J$ is comparable to the the
 194 characteristic wave length λ_c from the experiments.
 195

196 Some intuition for how Eq. (1) produces different dynamics
 197 on either side of the ADC can be gained by considering the
 198 relative contributions of the cubic and quadratic terms to the
 199 Hamiltonian \mathcal{H}_Λ^\pm . The depth change, $D_+ < 1$, increases the
 200 weight of H_3 and decreases that of H_2 , thus promoting the
 201 effects of nonlinearity and reducing dispersion. Since $\frac{\partial u}{\partial x}$ is
 202 the slope of the wave height, $H_2(u)$ measures the wave slope
 203 energy.

204 A *deterministic matching condition* is applied to the surface
 205 displacement u_Λ^\pm to link the incoming and outgoing wave trains.
 206 Assuming the abrupt depth change is met at $t = T_{\text{ADC}}$, the
 207 matching condition is given by

$$208 \quad u_\Lambda^-(x, t)|_{t=T_{\text{ADC}}^-} = u_\Lambda^+(x, t)|_{t=T_{\text{ADC}}^+},$$

209 Equation [1] is not designed to capture the short scale changes
 210 in rapid time. Rather, since we are interested in modeling
 211 statistics before and after the ADC, we will examine the long-
 212 time dynamics of large-scale structures.
 213

214 Interpreting experimental parameters in the dynamical model.

215 The model parameters (E_0, L_0, Λ) in [1] can be directly linked
 216 to the basic scales from the physical problem. The important
 217 characterizing parameters measured from the experiments
 218 include: $\epsilon = \frac{a}{H_0}$ the wave amplitude a to water depth H_0
 219 ratio; $\delta = \frac{H_0}{\lambda_c}$ the water depth to wavelength scale λ_c ratio;
 220 and $D_0 = \frac{d}{H_0}$ the normalized wave depth ratio with incoming
 221 flow depth $d = H_0$ to the outgoing flow depth $d < H_0$. The
 222 interpretations and reference values of these model parameters
 223 are based on the experimental setup (20). By comparing the
 224 characteristic physical scales, the normalized TKdV equation
 225 [1] can be linked directly with the measured non-dimensional
 226 quantities by

$$227 \quad L_0 = 6^{\frac{1}{3}} \left(M \epsilon^{\frac{1}{2}} \delta^{-1} \right), \quad E_0 = \frac{27}{2} \gamma^{-2} \left(M \epsilon^{\frac{1}{2}} \delta^{-1} \right), \quad [2]$$

228 where M defines the computational domain size $M\lambda_c$ as M -
 229 multiple of the characteristic wavelength λ_c , and $\gamma = \frac{U}{a}$ rep-
 230 presents the factor to normalize the total energy in the state
 231 variable u_Λ to one.
 232

233 Consider the spatial discretization $J = 2\Lambda + 1$ so that the
 234 smallest resolved scale is comparable with the characteristic
 235 wavelength

$$236 \quad \Delta x = \frac{2\pi M \lambda_c}{J} \lesssim \lambda_c \Rightarrow M = \frac{J}{2\pi} \sim 5, \quad J = 32.$$

237 Therefore in the practical numerical simulations, we pick
 238 $M = 5$ and γ varies in the range $[0.5, 1]$. Using the reference
 239 experimental measurements (20), $\epsilon \in [0.0024, 0.024]$, $\delta \sim 0.22$,
 240 and D_0 changes from 1 to 0.24 before and after the depth
 241 change. The reference values for the model scales can be esti-
 242 mated in the range $L_0 \in [2, 6]$ and $E_0 \in [50, 200]$. These are
 243 the values we will test in the direct numerical simulations. See
 244 details about the derivation from scale analysis in *SI Appendix*,
 245 *A*.

<p>249 3. Equilibrium statistical mechanics for generating the 250 stationary invariant measure</p> <p>252 Since the TKdV equation satisfies the Liouville property, the 253 equilibrium invariant measure can be described by an equi- 254 librium statistical formulism (24–26) using a Gibbs measure 255 with the conserved energy \mathcal{E}_Λ and Hamiltonian \mathcal{H}_Λ. The equi- 256 librium invariant measure is dictated by the conservation laws 257 in the TKdV equation. In the case with fixed total energy E_0, 258 this is the <i>mixed Gibbs measure</i> in the truncated model with 259 microcanonical energy and canonical Hamiltonian ensembles 260 (24)</p> <p>261 $\mathcal{G}_\theta^\pm(u_\Lambda^\pm; E_0) = C_\theta^\pm \exp(-\theta^\pm \mathcal{H}(u_\Lambda^\pm)) \delta(\mathcal{E}(u_\Lambda^\pm) - E_0),$ [3]</p> <p>262 with θ representing the “inverse temperature”. The distinct 263 statistics in the upstream and downstream waves can be con- 264 trolled by the value of θ. Negative temperature, $\theta^\pm < 0$, is 265 the appropriate regime to predict the experiments as shown 266 below. In the incoming flow field, the inverse temperature θ^- 267 is chosen so that \mathcal{G}_θ^- has Gaussian statistics. Using the above 268 invariant measures [3], the expectation of any functional $F(u)$ 269 can be computed based on the Gibbs measure</p> <p>270</p> <p>271 $\langle F \rangle_{\mathcal{G}_\theta} \equiv \int F(u) \mathcal{G}_\theta(u) du.$</p> <p>272</p> <p>273 The value of θ in the invariant measure is specified from $\langle H_\Lambda \rangle_{\mathcal{G}_\theta}$ 274 (24, 26). The invariant measure also predicts an equilibrium 275 energy spectrum without running the TKdV equation directly. 276 On the other hand, the time autocorrelation and transient 277 statistics about the state variable u_Λ cannot be recovered from 278 the statistical theory.</p> <p>279</p> <p>280 Statistical matching condition in invariant measures before 281 and after the abrupt depth change. The Gibbs measures \mathcal{G}_θ^\pm 282 are defined based on the different inverse temperatures θ^\pm on 283 the two sides of the solutions</p> <p>284</p> <p>285 $\begin{aligned} \mu_t^-(u_\Lambda^-; D_-), \quad u_\Lambda _{t=T_{ADC}-} &= u_0, \quad t < T_{ADC}; \\ \mu_t^+(u_\Lambda^+; D_+), \quad u_\Lambda _{t=T_{ADC}+} &= u_0, \quad t > T_{ADC}, \end{aligned}$</p> <p>286 where u_0 represents the deterministic matching condition be- 287 tween the incoming and outgoing waves. The two distributions, 288 μ_t^-, μ_t^+ should also be matched at the depth change location 289 T_{ADC}, so that,</p> <p>290</p> <p>291 $\mu_{t=T_{ADC}}^-(u_\Lambda) = \mu_{t=T_{ADC}}^+(u_\Lambda).$</p> <p>292</p> <p>293 In matching the flow statistics before and after the abrupt 294 depth change, we first use the conservation of the determinis- 295 tic Hamiltonian H_Λ^+ after the depth change. Then assuming 296 ergodicity (24, 25), the statistical expectation for the Hamil- 297 tonian $\langle H_\Lambda^+ \rangle$ is conserved in time after the depth change at 298 $t = T_{ADC}$ and should stay in the same value as the system ap- 299 proaches equilibrium as $t \rightarrow \infty$. The final statistical matching 300 condition to get the outgoing flow statistics with parameter 301 θ^+ can be found by</p> <p>302</p> <p>303 $\langle H_\Lambda^+ \rangle_{\mathcal{G}_\theta^+} = \langle H_\Lambda^+ \rangle_{\mathcal{G}_\theta^-},$ [4]</p> <p>304 with the outgoing flow Hamiltonian H_Λ^+ and the Gibbs mea- 305 sures \mathcal{G}_θ^\pm before and after the abrupt depth change.</p>	<p>4. The nearly Gaussian incoming statistical state</p> <p>The incoming flow is always characterized by a near-Gaussian distribution in the wave displacement. It is found that a physically consistent Gibbs measure should take negative values in the inverse temperature parameter $\theta < 0$, where a proper distribution function and a decaying energy spectrum are generated (see (26) and <i>SI Appendix, B.1</i> for the explicit simulation results). The upstream Gibbs measure \mathcal{G}_θ^- with $D_- = 1$ displays a wide parameter regime in (θ^-, E_0) with near-Gaussian statistics. In the left panel of Figure 1 (a), the inflow skewness κ_3^- varies only slightly with changing values of E_0 and θ^-. The incoming flow PDF then can be determined by picking the proper parameter value θ^- in the near Gaussian regime with small skewness. In contrast, the downstream Gibbs measure \mathcal{G}_θ^+ with $D_+ = 0.24$ shown in the right panel of Figure 1 (a) generates much larger skewness κ_3^+ as the absolute value of θ^+ and the total energy level E_0 increases. The solid lines in Figure 1 (c) offer a further confirmation of the transition from near-Gaussian statistics with small κ_3^- to a strongly skewed distribution κ_3^+ after the depth change.</p> <p>In the next step, the value of the downstream θ^+ is determined based on the matching condition [4]. The expectation $\langle H_\Lambda^+ \rangle_{\mathcal{G}_\theta^-}$ about the incoming flow Gibbs measure can be calculated according to the predetermined parameter values of θ^- as well as E_0 from the previous step. For the direct numerical experiments shown later in Figure 2, we pick proper choices of test parameter values as $L_0 = 6, E_0 = 100$ and $\theta^- = -0.1, -0.3, -0.5$. More test cases with different system energy E_0 can be found in <i>SI Appendix, B.2</i> where similar transition from near Gaussian symmetric PDFs to skewed PDFs in the flow state u_Λ^\pm can always be observed.</p> <p>Direct numerical model simulations. Besides the prediction of equilibrium statistical measures from the equilibrium statistical approach, another way to predict the downstream model statistics is through running the dynamical model [1] directly. The TKdV equation is found to be ergodic with proper mixing property as measured by the decay of autocorrelations as long as the system starts from a negative inverse temperature state as described before. For direct numerical simulations of the TKdV equations, a proper symplectic integrator is required to guarantee the Hamiltonian and energy are conserved in time. It is crucial to use the symplectic scheme to guarantee the exact conservation of the energy and Hamiltonian since they are playing the central role in generating the invariant measure and the statistical matching. The symplectic schemes used here for the time integration of the equation is the 4th-order midpoint method (27). Details about the mixing properties from different initial states and the numerical algorithm are described in <i>SI Appendix, C</i>.</p> <p>5. Predicting extreme anomalous behavior after the ADC by statistical matching</p> <p>With the inflow statistics well described and the numerical scheme set up, we are able to predict the downstream anomalous statistics starting from the near-Gaussian incoming flow going through the abrupt depth change from $D_- = 1$ to $D_+ = 0.24$. First, we consider the statistical prediction in the downstream equilibrium measure directly from the matching condition. The downstream parameter value θ^+ is determined</p>
---	--

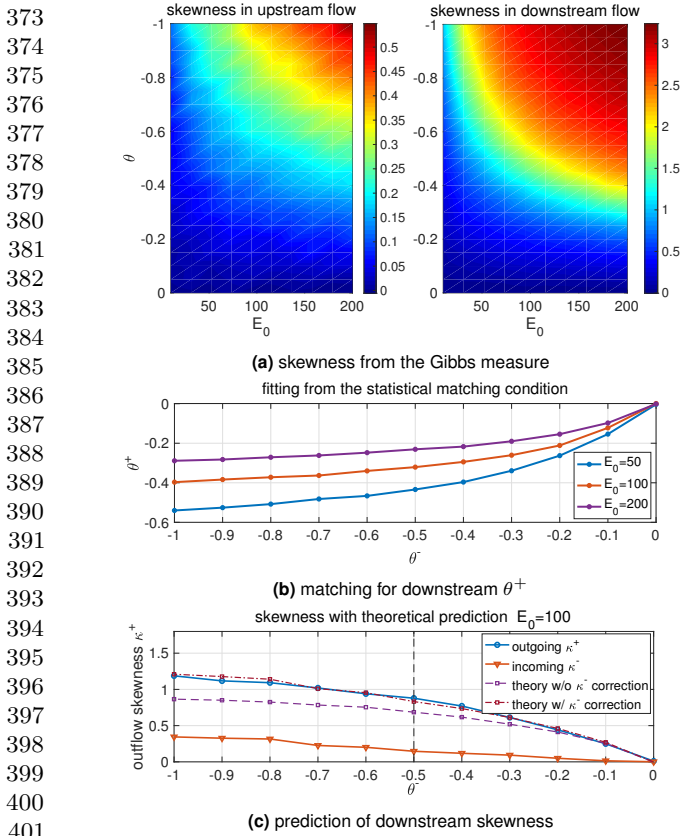


Fig. 1. First row: skewness from the Gibbs measures in incoming and outgoing flow states with different values of total energy E_0 and inverse temperature θ (notice the different scales in the incoming and outgoing flows); Second row: outgoing flow parameter θ^+ as a function of the incoming flow θ^- computed from the statistical matching condition with three energy level E_0 ; Last row: skewness in the outgoing flow with the matched value of θ^+ as a function of the inflow parameter θ^- (the theoretical predictions using [5] are compared).

by solving the nonlinear equation [4] as a function of θ^+ , $F(\theta^+) = \langle H_\Lambda^+ \rangle_{\mathcal{G}_\theta^+}(\theta^+) - \langle H_\Lambda^+ \rangle_{\mathcal{G}_\theta^-} = 0$. In the numerical approach, we adopt a modified secant method avoiding the stiffness in the parameter regime (see the *SI Appendix, B.2* for the algorithm). The fitted solution is plotted in Figure 1 (b) as a function of the proposed inflow θ^- . A nonlinear $\theta^- - \theta^+$ relation is discovered from the matching condition. The downstream inverse temperature θ^+ will finally saturate at some level. The corresponding downstream skewness of the wave displacement u_Λ predicted from the statistical matching of Gibbs measures is plotted in Figure 1 (c). In general, a large positive skewness for outgoing flow κ_3^+ is predicted from the theory, while the incoming flow skewness κ_3^- is kept in a small value in a wide range of θ^- . Note that with $\theta^- \sim 0$ (that is, using the microcanonical ensemble only with energy conservation), the outflow statistics are also near Gaussian with weak skewness. The skewness in the outflow statistics grows as the inflow parameter value θ^- increases in amplitude.

For a second approach, we can use direct numerical simulations starting from the initial state sampled from the incoming flow Gibbs measure \mathcal{G}_θ^- and check the transient changes in the model statistics. Figure 2 illustrates the change of statistics as the flow goes through the abrupt depth change. The first row plots the changes in the skewness and kurtosis for the

state variable u_Λ after the depth change at $t = 0$. The PDFs in the incoming and outgoing flow states are compared with three different initial inverse temperatures θ^- . After the depth changes to $D_0 = 0.24$ abruptly at $t = 0$, both the skewness and kurtosis jump to a much larger value in a short time, implying the rapid transition to a highly skewed non-Gaussian statistical regime after the depth change. Further from Figure 2, different initial skewness (but all relatively small) is set due to the various values of θ^- . With small $\theta^- = -0.1$, the change in the skewness is not very obvious (see the second row of Figure 2 for the incoming and outgoing PDFs of u_Λ). In comparison, if the incoming flow starts from the initial parameter $\theta^- = -0.3$ and $\theta^- = -0.5$, much larger increase in the skewness is induced from the abrupt depth change. Furthermore, in the detailed plots in the third row of Figure 2 for the downstream PDFs under logarithmic scale, fat tails towards the positive direction can be observed, which represent the extreme events in the downstream flow (see also Figure 3 for the time-series of u_Λ).

As a result, the downstream statistics in final equilibrium predicted from the direct numerical simulations here agree with the equilibrium statistical mechanics prediction illustrated in Figure 1. The prediction from these two different approaches confirm each other.

6. Analytic formula for the upstream skewness after the ADC

A statistical link between the upstream and downstream energy spectra can be found for an analytical prediction of the skewness in the flow state u after the ADC. The skewness of the state variable u_j at one spatial grid point is defined as the ratio between the third and second moments

$$\kappa_3 = \langle u_j^3 \rangle_\mu / \langle u_j^2 \rangle_\mu^{3/2}.$$

Now we introduce mild assumptions on the distribution functions:

- The upstream equilibrium measure μ_- has a relatively small skewness so that

$$\langle H_3 \rangle_{\mu_-} = \frac{1}{6} \int_{-\pi}^{\pi} \langle u^3 \rangle_{\mu_-} dx \equiv \epsilon;$$

- The downstream equilibrium measure μ_+ is homogeneous at each physical grid point, so that the second and third moments are invariant at each grid point

$$\langle u_j^2 \rangle_{\mu_+} = \sigma^2 = \pi^{-1}, \quad \langle u_j^3 \rangle_{\mu_+} = \sigma^3 \kappa_3 = \pi^{-3/2} \kappa_3^+.$$

Then the skewness of the downstream state variable u_Λ^+ after the ADC is given by the difference between the inflow and outflow wave slope energy of u_x

$$\kappa_3^+ = \frac{3}{2} \pi^{1/2} L_0^{-3/2} E_0^{-1/2} D_+^2 \int_{-\pi}^{\pi} [\langle u_x^2 \rangle_{\mu_+} - \langle u_x^2 \rangle_{\mu_-}] dx + 3\pi^{1/2} \epsilon. \quad [5]$$

The detailed derivation is shown in *SI Appendix, B.2*. In particular, the downstream skewness with near-Gaussian inflow statistics $\epsilon \ll 1$ is positive if and only if the difference of the incoming and outgoing wave slope energy is positive. This

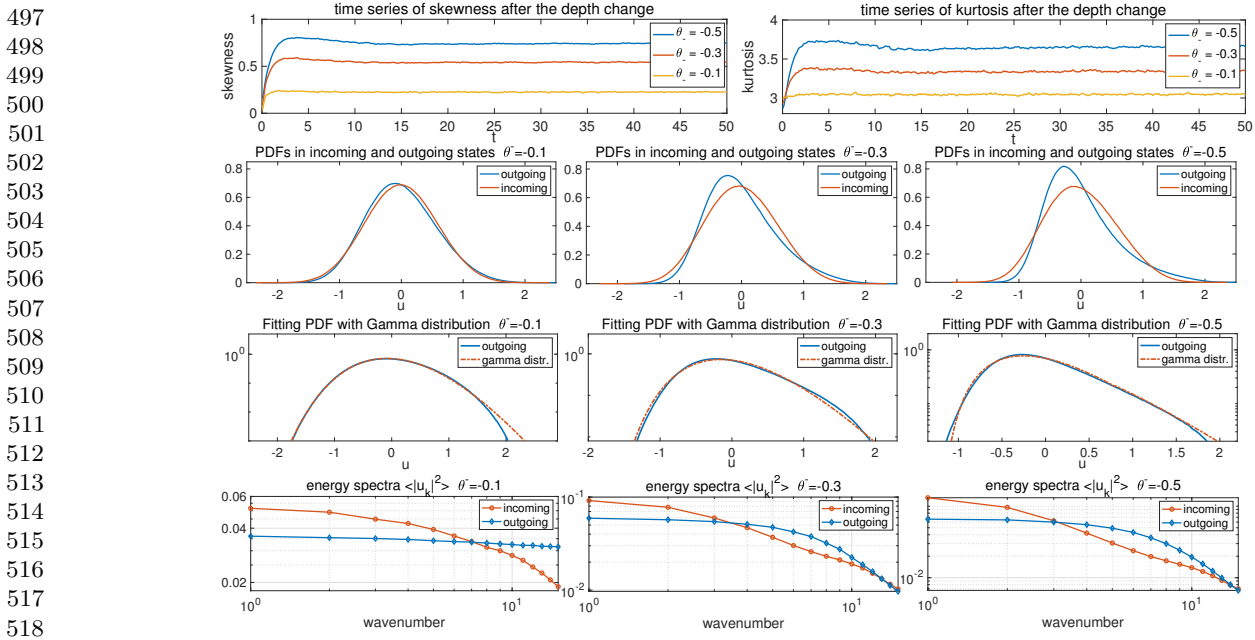


Fig. 2. Changes in the statistics of the flow state going through the abrupt depth change. The initial ensemble is set with the incoming flow Gibbs measure with different inverse temperature θ^- . First row: time evolution of the skewness and kurtosis. The abrupt depth change is taking place at $t = 0$; Second row: inflow and outflow PDFs of u_Λ ; Third row: the downstream PDFs fitted with Gamma distributions with consistent variance and skewness (in log coordinate in y); Last row: energy spectra in the incoming and outgoing flows.

523

524

means that there is more small scale wave slope energy in the outgoing state. As an evidence, in the last row of Figure 2 in all the weak and strong skewness cases, the outflow energy spectrum always has a slower decay rate than the inflow energy spectrum which possesses stronger energy in larger scales and weaker energy in the smaller scales.

In Figure 1 (c), we compare the accuracy of the theoretical estimation [5] with numerical tests. In the regime with small incoming inverse temperature θ^- , the theoretical formula offers a quite accurate approximation of the third-order skewness using only information from the second-order moments of the wave-slope spectrum.

7. Key features from experiments captured by the statistical dynamical model

In this final section, we emphasize the crucial features generated by the statistical dynamical model [1] by making comparison with the experimental observations in (20). As from the scale analysis displayed in Section 2, the theory is set in the same parameter regime as the experimental setup.

- The transition from near-Gaussian to skewed non-Gaussian distribution as well as the jump in both skewness and kurtosis observed in the experiment observations (Fig. 1 of (20)) can be characterized by the statistical model simulation results (see the first and second row of Figure 2). Notice that the difference in the decay of third and fourth moments in the far end of the downstream regime from the experimental data is due to the dissipation effect in the flow from the wave absorbers that is not modeled in the statistical model here. The model simulation time-series plotted in Figure 3 can be compared with the observed time sequences from experiments (Fig. 1 of (20)). The downstream simulation generates waves with

strong and frequent intermittency towards the positive displacement, while the upstream waves show symmetric displacements in two directions with at most small peaks in slow time. Even in the time-series at a single location $x = 0$, the long-time variation displays similar structures.

- The downstream PDFs in experimental data are estimated with a Gamma distribution in Fig. 2 of (20). Here in the same way, we can fit the highly skewed outgoing flow PDFs from the numerical results with the Gamma distribution

$$\rho(u; k, \alpha) = \frac{e^{-k} \alpha^{-1}}{\Gamma(k)} (k + \alpha^{-1} u)^{k-1} e^{-\alpha^{-1} u}.$$

The parameters (k, α) in the Gamma distribution are fitted according to the measured statistics in skewness and variance, that is, $\sigma^2 = k\alpha^2$, $\kappa_3 = 2/\sqrt{k}$. And the excess kurtosis of the Gamma distribution can be recovered as $\kappa_4 = 6/k$. As shown in the third row of Figure 2, excellent agreement in the PDFs with the Gamma distributions is reached in consistency with the experimental data observations. The accuracy with this approximation increases as the initial inverse temperature θ^- increases in value to generate more skewed distribution functions.

- The experiments also have the up and down stream power spectra in time (Fig. 4 of (20)), which shows more energy at small time scales, i.e., a relatively slower decay rate in the downstream compared with the upstream case. This is also observed in the direct numerical simulations here (detailed results shown in *SI Appendix, C.2*). The downstream state contains more energetic high frequencies. **The peak frequency illustrates the characteristic time scale of the transporting wave trains along the water tank.**

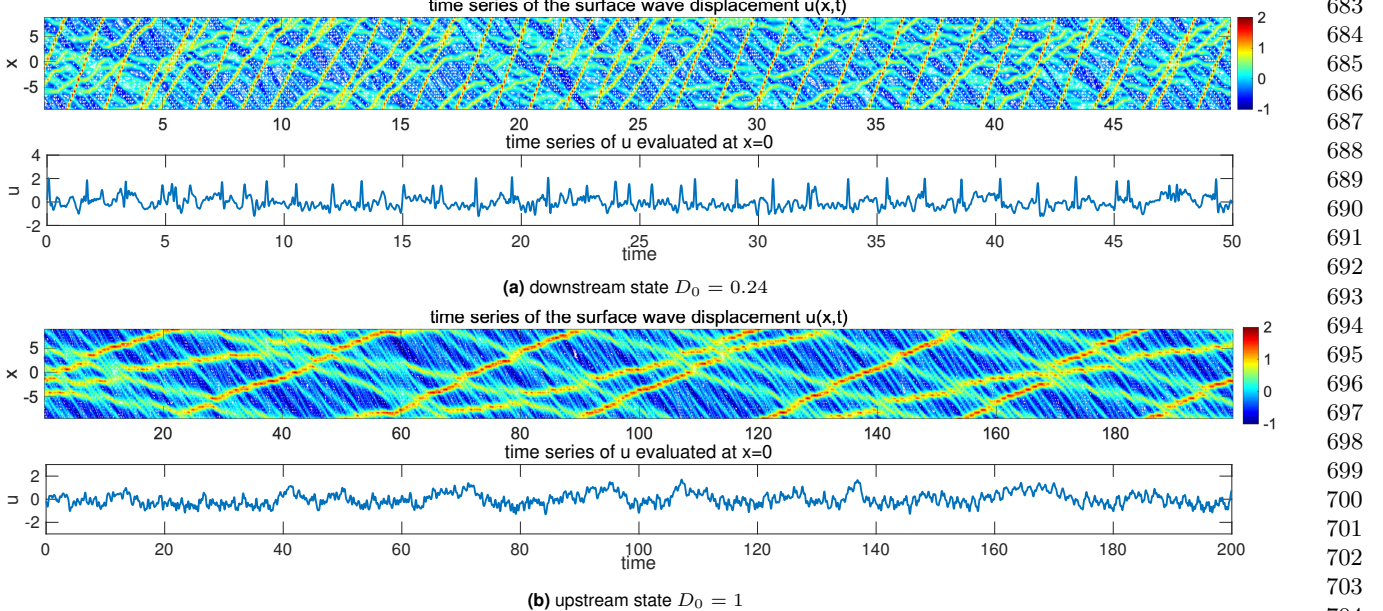


Fig. 3. Realization of the downstream and upstream flow solutions u_A^\pm . Note the larger vertical scale in the downstream time-series plot.

I do not understand the last sentence above. Why does the peak frequency illustrate the occurrence of transporting water waves?

8. Concluding discussion

We have developed a statistical dynamical model to explain and predict extreme events and anomalous features of shallow water waves crossing an abrupt depth change. The theory is based on the dynamical modeling strategy consisting of the TKdV equation matched at the abrupt depth change with conservation of energy and Hamiltonian. Predictions can be made of the extreme events and anomalous features by matching incoming and outgoing statistical Gibbs measures before and

after the abrupt depth transition. The statistical matching of the known nearly Gaussian incoming Gibbs state completely determines the predicted anomalous outgoing Gibbs state, which can be calculated by a simple sampling algorithm, verified by direct numerical simulations, and successfully captures key features of the experiment. An analytic formula for the anomalous outgoing skewness is also derived. The strategy here should be useful for predicting extreme statistical events in other dispersive media in different settings.

ACKNOWLEDGMENTS. This research of A. J. M. is partially supported by the Office of Naval Research through MURI N00014-16-1-2161. D. Q. is supported as a postdoctoral fellow on the second grant. M.N.J.M would like to acknowledge support from Simons grant 524259.

1. Majda AJ, Branicki M (2012) Lessons in uncertainty quantification for turbulent dynamical systems. *Discrete & Continuous Dynamical Systems-A* 32(9):3133–3221.
2. Mohamad MA, Sapsis TP (2018) A sequential sampling strategy for extreme event statistics in nonlinear dynamical systems. *Proceedings of the National Academy of Sciences* 115(44):11138–11143.
3. Qi D, Majda AJ (2016) Predicting fat-tailed intermittent probability distributions in passive scalar turbulence with imperfect models through empirical information theory. *Communications in Mathematical Sciences* 14(6):1687–1722.
4. Majda AJ, Tong XT (2015) Intermittency in turbulent diffusion models with a mean gradient. *Nonlinearity* 28(11):4171–4208.
5. Majda AJ, Chen N (2018) Model error, information barriers, state estimation and prediction in complex multiscale systems. *Entropy* 20(9):644.
6. Majda AJ, Tong XT (2018) Simple nonlinear models with rigorous extreme events and heavy tails. *arXiv preprint arXiv:1805.05615*.
7. Thual S, Majda AJ, Chen N, Stechmann SN (2016) Simple stochastic model for el nino with westerly wind bursts. *Proceedings of the National Academy of Sciences* 113(37):10245–10250.
8. Chen N, Majda AJ (2018) Efficient statistically accurate algorithms for the Fokker-Planck equation in large dimensions. *Journal of Computational Physics* 354:242–268.
9. Chen N, Majda AJ (2017) Beating the curse of dimension with accurate statistics for the Fokker-Planck equation in complex turbulent systems. *Proceedings of the National Academy of Sciences* 114(49):12864–12869.
10. Chen N, Majda AJ (2018) Conditional Gaussian systems for multiscale nonlinear stochastic systems: Prediction, state estimation and uncertainty quantification. *Entropy* 20(7):509.
11. Qi D, Majda AJ (2018) Predicting extreme events for passive scalar turbulence in two-layer baroclinic flows through reduced-order stochastic models. *Communications in Mathematical Sciences* 16(1):17–51.
12. Adcock TA, Taylor PH (2014) The physics of anomalous ('rogue') ocean waves. *Reports on Progress in Physics* 77(10):105901.
13. Cousins W, Sapsis TP (2015) Unsteady evolution of localized unidirectional deep-water wave groups. *Physical Review E* 91(6):063204.
14. Farazmand M, Sapsis TP (2017) Reduced-order prediction of rogue waves in two-dimensional deep-water waves. *Journal of Computational Physics* 340:418–434.
15. Onorato M, Osborne AR, Serio M, Bertone S (2001) Freak waves in random oceanic sea states. *Physical Review Letters* 86(25):5831–5834.
16. Demattei G, Grafke T, Vanden-Eijnden E (2018) Rogue waves and large deviations in deep sea. *Proceedings of the National Academy of Sciences* 115(5):855–860.
17. Sergeeva A, Pelinovsky E, Talipova T (2011) Nonlinear random wave field in shallow water: variable Korteweg-de Vries framework. *Natural Hazards and Earth System Sciences* 11(2):323–330.
18. Trulsen K, Zeng H, Gramstad O (2012) Laboratory evidence of freak waves provoked by non-uniform bathymetry. *Physics of Fluids* 24(9):097101.
19. Viotti C, Dias F (2014) Extreme waves induced by strong depth transitions: Fully nonlinear results. *Physics of Fluids* 26(5):051705.
20. Bolles CT, Speer K, Moore MNJ (2018) Anomalous wave statistics induced by abrupt depth change. *arXiv preprint arXiv:1808.07958*.
21. Solli D, Ropers C, Koonath P, Jalali B (2007) Optical rogue waves. *Nature* 450(7172):1054.
22. Höhmann R, Kuhl U, Stöckmann HJ, Kaplan L, Heller E (2010) Freak waves in the linear regime: A microwave study. *Physical review letters* 104(9):093901.
23. Johnson RS (1997) *A modern introduction to the mathematical theory of water waves*. (Cambridge university press) Vol. 19.
24. Abramov RV, Kováčik G, Majda AJ (2003) Hamiltonian structure and statistically relevant conserved quantities for the truncated Burgers-Hopf equation. *Communications on Pure and Applied Mathematics: A Journal Issued by the Courant Institute of Mathematical Sciences* 56(1):1–46.
25. Majda A, Wang X (2006) *Nonlinear dynamics and statistical theories for basic geophysical flows*. (Cambridge University Press).
26. Bajars J, Frank J, Leimkuhler B (2013) Weakly coupled heat bath models for Gibbs-like invariant states in nonlinear wave equations. *Nonlinearity* 26(7):1945–1973.
27. McLachlan R (1993) Symplectic integration of hamiltonian wave equations. *Numerische Mathematik* 66(1):465–492.